J Mater Sci (2009) 44:306–315
DOI 10.1007/s10853-008-3053-8

Effects of atmospheric corrosion on fatigue properties of a medium carbon steel

M. Okayasu · K. Sato · K. Okada · S. Yoshifuji · M. Mizuno

Received: 29 October 2007 / Accepted: 15 October 2008 / Published online: 10 November 2008

Abstract The effects of atmospheric corrosion on fatigue properties were examined using a medium carbon steel, corroded in various atmospheres. Three different places, having various atmospheric conditions, were selected for the corrosion tests: (i) an industrial area, (ii) near the ocean, and (iii) beside a river in a hot spring region. A water and/or air electrochemical cell corroded the carbon steel to rust that had several forms, depending on the atmosphere. The form of the corrosion was distinguished visually and by spectroscopy. Strong oxidation occurred in all samples with the formation of rust. In addition, a more severe chemical reaction with chlorine was detected near the ocean although carbon was obtained in the industrial area. On the other hand, a high level of sulfur reacted with the sample near the river. Such chemical reactions gave rise to different corrosion mechanisms leading to different corrosion surfaces. A rough corrosion face with corrosion pits was obtained in two of the samples (industrial area and near the ocean), while a smooth surface was produced for the sample near the river. The change of the surface morphology clearly affected the fatigue strength, e.g., the rougher the sample surface, the lower the fatigue strength. On the basis of the corrosion system, details of the fracture and fatigue characteristics are discussed in the present work.

M. Okayasu (✉) · K. Sato · S. Yoshifuji · M. Mizuno
Department of Machine Intelligence and Systems Engineering, Akita Prefectural University, 84-4 Ebinokuchi, Tuchiya-aza, Yurihonjo-city, Akita 015-0055, Japan
e-mail: okayasu@akita-pu.ac.jp

K. Okada
Akita Prefectural R&D Center, 4-21 Sanuki, Araya, Akita-city, Akita 010-1623, Japan

Introduction

Corrosion of materials due to the influence of the environment frequently occurs in structures and their components despite the use of corrosion protection systems. This can be observed as the corrosion protection and prevention systems are consumed. Severe corrosion in some materials can reduce their fatigue and mechanical strengths. In recent years, fractures have occurred in various structures in Japan due to metallic corrosion. For instance, (i) iron pipes for CH_4 gas were cracked open by the atmosphere corrosion and the gas widely spread in the neighborhood and (ii) a cradle swing in a playground, made of carbon steels, completely collapsed. Carbon steels exposed to oxygen in the atmosphere rapidly form a superficial oxide layer, and this can change the material properties [1–4]. Because the fatigue performance is of great significance in the assessment of structural integrity, the corrosion-fatigue properties of carbon steels have been examined by several investigators; it appeared that the material strength was significantly reduced by the metal corrosion. The crack growth characteristic is changed in a corrosion-fatigue test, especially (i) crack initiation and (ii) crack growth stage [5].

Crack initiation occurs by the following mechanism: the corrosion on the main slip plane, e.g., {111}, causes a high shear stress on the plane, resulting in a dislocation movement [6]. Another mechanism to be considered is intergranular stress corrosion cracking. Fukuzumi et al. reported that the intergranular fracture surface is created in spring steel corroded by NaCl vapor [3] because of hydrogen embrittlement. The corrosion-fatigue crack growth characteristics have also been examined by several researchers [7–15]. In these reports, the specimen materials were exposed to water vapor with NaCl or Na_2SO_4. It was

established that the fatigue crack growth rate can either slow down or accelerate during the fatigue test, depending on the corrosion mechanism. It appeared that a corrosion product inducing a wedge effect, i.e., crack closure, decreases the rate of crack growth [7, 8]. The wedge effect was especially influential at a frequency $f = 5$ Hz, but became weak at frequencies of the order of 0.1 Hz and 0.01 Hz [7]. A related approach was conducted using titanium alloys, in which the ΔK_{eff} level was reduced by the corrosion products generated on the crack surfaces [9]. On the other hand, the crack growth rate accelerates when a rough specimen surface, such as corrosion pits, is created, [10–12].

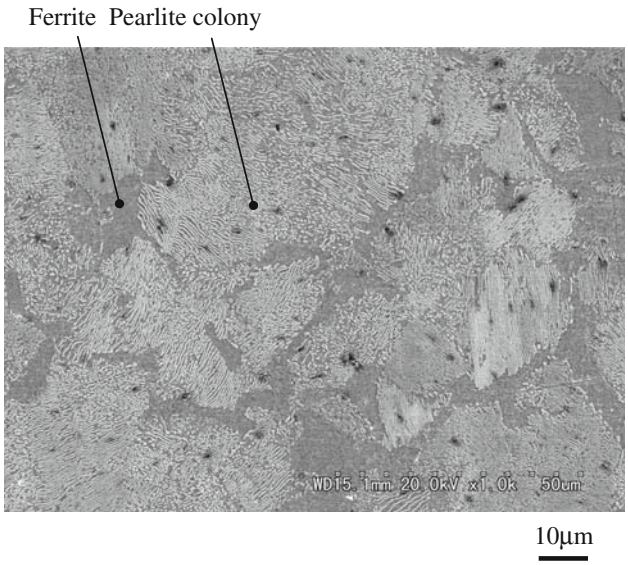

Fig. 1 Micrograph of the medium carbon steel (0.45%C) showing ferrite and pearlite colonies

From the above literature survey, it was found that crack growth characteristics depend on the corrosion criterion. In the study by several researchers, corrosion-fatigue tests have been carried out using various metals artificially corroded via the vapor corrosion test. One of the advantages of the vapor test is that it causes the metal corrosion in a short period of time even though the corrosion characteristics may not be exactly the same as those found in the natural corrosion situation. Establishing the atmospheric corrosion-fatigue properties of structural metals could provide more reliable data for the design of structures and components. The aim of this research is, therefore, to investigate the atmospheric corrosion-fatigue properties of medium carbon steels. In the present study,

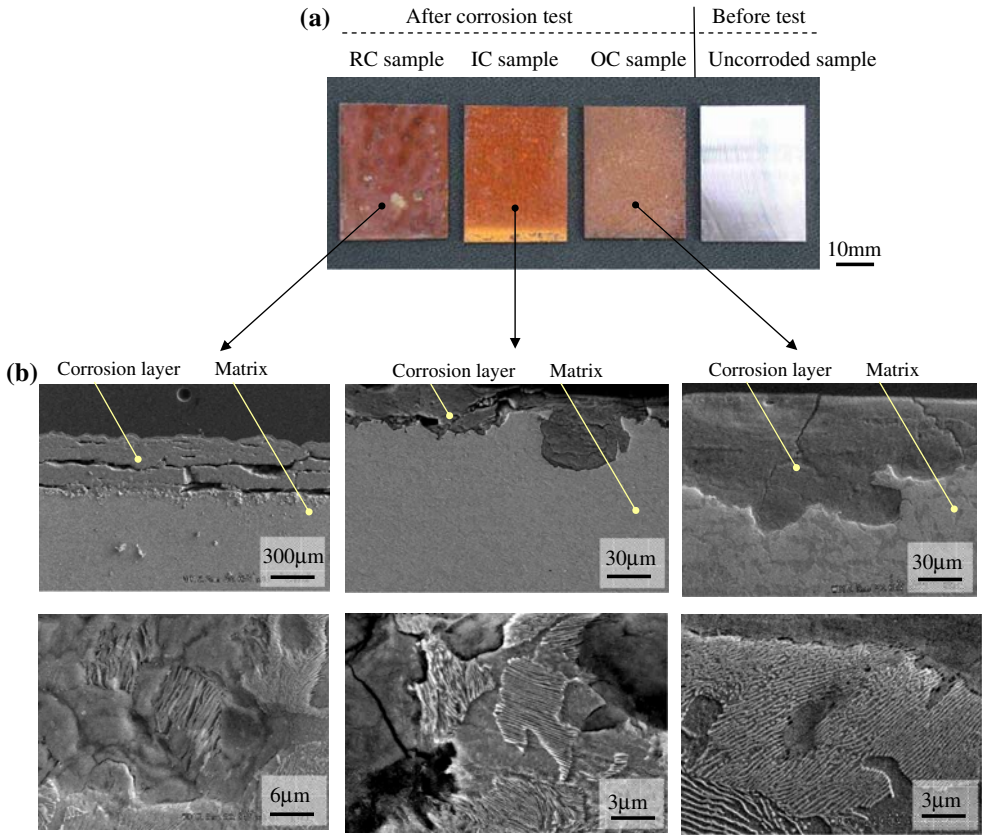

Fig. 2 **a** Surface of the specimen before and after the corrosion test and **b** Cross section of specimen near the corrosion layer: RC (beside the river in the hot spring region), IC sample (the industrial area), and OC (near the ocean)

we have chosen three different sites with different typical atmospheric conditions.

Material and experimental procedures

Specimen material

The material selected in this investigation is a commercial hot-rolled medium carbon steel, supplied in the form of 12.7-mm thick flat bars. The chemical composition of the carbon steel is (wt%): 0.45 C, 0.76 Mn, <0.01 P, <0.01 S, balanced with Fe. The material was first annealed at 923 K for 2 h, and cooled in air to remove the residual stresses. Figure 1 shows the microstructure of the carbon steel after the annealing process, showing it to consist of regular ferrite and pearlite with a mean grain size of 25 μm in diameter. The tensile properties of the steel at room temperature are: tensile strength $\sigma_{UTS} = 638$ MPa, yield strength $\sigma_y = 382$ MPa, and elongation to fracture $\gamma = 25\%$.

Atmospheric corrosion tests

Atmospheric corrosion tests were carried out at three locations in Japan: (i) in an industrial area (IC), (ii) near the ocean (OC), and (iii) beside the river in a hot spring region (RC). The detailed locations for the three test places are: (i) IC: Kitakasai, Edogawa-ward, Tokyo; (ii) OC: Honjo marina, Yurihonjo-city, Akita; and (iii) RC: Tamagawa hot spring, Senboku-city, Akita. The three places were selected because of their different atmospheric conditions: (i) air pollution arising from automobiles and factories in IC; (ii) sea breezes in OC; and (iii) water vapor from the hot springs in RC. In this test, the carbon steel was machined into flat plates with $B = 50$ mm, $H = 80$ mm, and $T = 5$ mm. The specimen shape was designed on the basis of the Japan Industrial Standard (JIS). The corrosion test was conducted over 3 months in the summer season from July to September 2005.

Bending and fatigue tests

The effects of atmospheric corrosion on the mechanical and fatigue properties were examined. In this case, three point bending specimens, with $b = 5$ mm, $h = 5$ mm, and $l = 50$ mm, were employed. Bending and fatigue tests were performed using an electro-servo-hydraulic system with 100 KN capacity. During the tests, the applied load and deflection value were monitored via a data acquisition system in conjunction with computer. The loading speed in the bending test was 1 mm/min. The cyclic loading in the fatigue test was conducted at a ratio, R, of 0.3 ($R = P_{min}/P_{max}$) and a frequency of 15 Hz, under load control. The maximum cyclic load, P_{max}, was detected in the load range between 45% and 85% of the bending yield load, P_y. Note that the P_{max} values

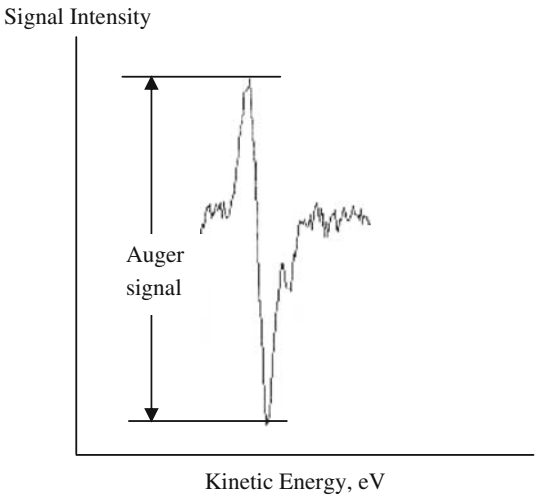

Fig. 3 Auger Electron Spectrometry showing the manner for the determination of the intensity of chemical element

Table 1 Signal intensities of chemical elements in the corrosion layer as detected by Auger Electron Spectrometry

Signal intensity	IC sample	OC sample	RC sample
O KLL	1 (12,302KLL)	1.05	1.0
C KLL	1 (1,032KLL)	0.75	0.8
S LVV	1	0.8	4.4 (1,890LVV)
Cl LVV	1	7.2 (720LVV)	1.0

The intensity is expressed as a ratio based on the level of the IC sample

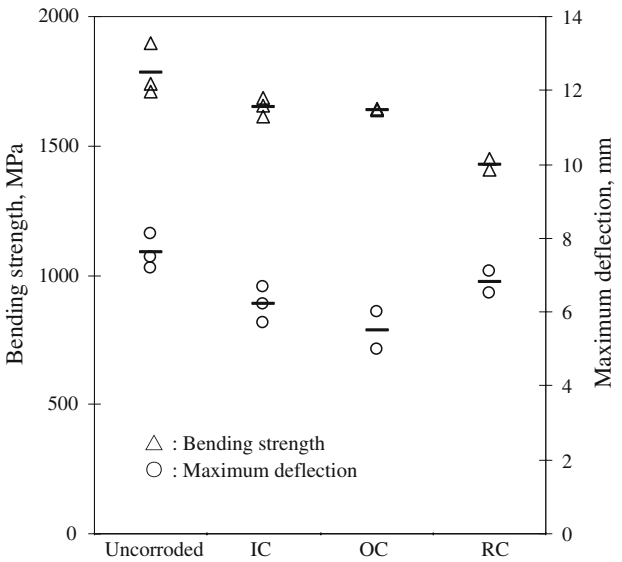

Fig. 4 Bending strength and maximum deflection for the uncorroded and corroded samples

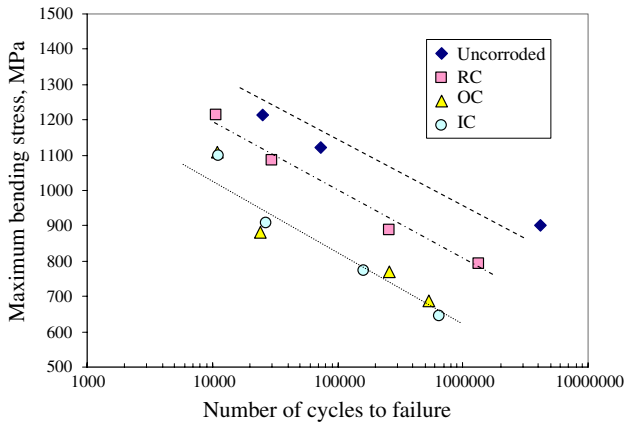

Fig. 5 S–N curves for the uncorroded and corroded samples

were chosen in response to the fact that plastic deformation in these samples does not occur, especially at the beginning of the fatigue tests. The stress amplitude was calculated using the following expression:

$$\sigma_a = \frac{3S}{2bh^2}(P_{\max} - P_{\min}) \quad (1)$$

where S is the loading span and b and h are the specimen width and height, respectively.

Finite element analysis

Finite element analysis (FEA) was used to analyze the stress–strain distribution in the sample during the cyclic loading. In this analysis, a two-dimensional finite element

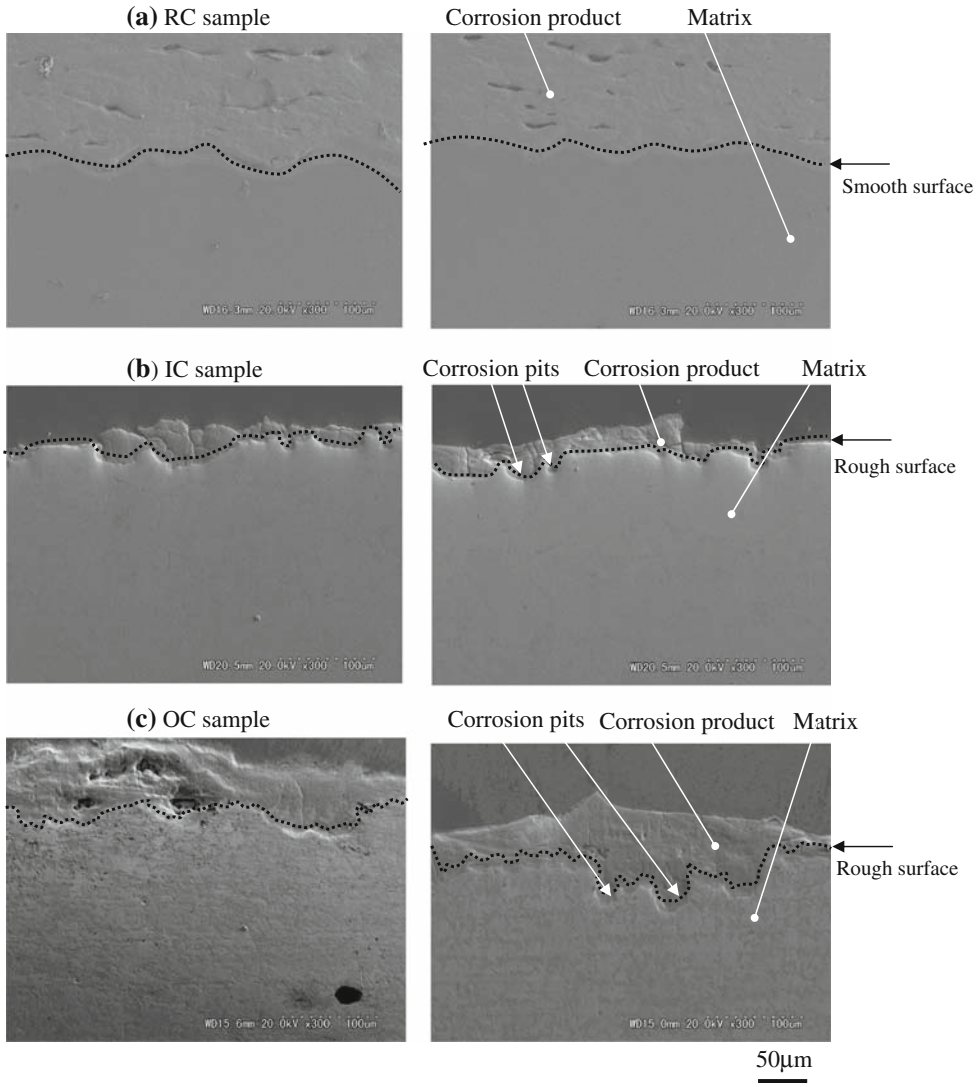

Fig. 6 SEM images of the cross section of the specimens near the corrosion products

simulation with 8-noded quad elements was employed. The FE models were designed according to the specimen geometry. The mesh size adjacent to the loading point was 0.05 mm. In this calculation, the case of bilinear kinematics hardening was selected. The material properties used in this analysis were: Young's modulus $E = 210$ GPa, yield stress $\sigma_y = 350$ MPa, and Poisson's ratio $v = 0.3$.

Results and discussion

Corrosion characteristics

The optical macrographs of the specimens before and after corrosion testing in the three different places are shown in Fig. 2a. It is clear that the surface color on the specimens after the corrosion test was altered. A reddish surface was seen in the IC sample (the industrial area), while light and dark brown colors were observed in the OC (near the ocean) and RC samples (beside the river in the hot spring region), respectively. Figure 2b shows the SEM images of the microstructure showing the cross section near the corrosion products. In the RC sample, a corrosion layer about 300 μm thick was obtained although much thinner layers (about 50 μm) appeared on the IC and OC specimens. These corrosion characteristics suggest different corrosion mechanisms.

To understand the material properties of the corrosion products, an Auger Electron Spectrometry (AES) analysis was carried out directly on the corrosion layer. In this case, the AES signal intensity was assessed by the range between the maximum and minimum signal levels, as shown in Fig. 3. The AES intensity levels obtained are indicated in Table 1, relative to the AES signal level of the IC sample. A high level of oxygen AES (12302KLL) at 512 eV was detected for all samples. This result may imply that a water-based substance corrodes the carbon steel, e.g., $Fe^{2+}+2H_2O = Fe(OH^+)_2 + 2H^+$, with anodic dissolution

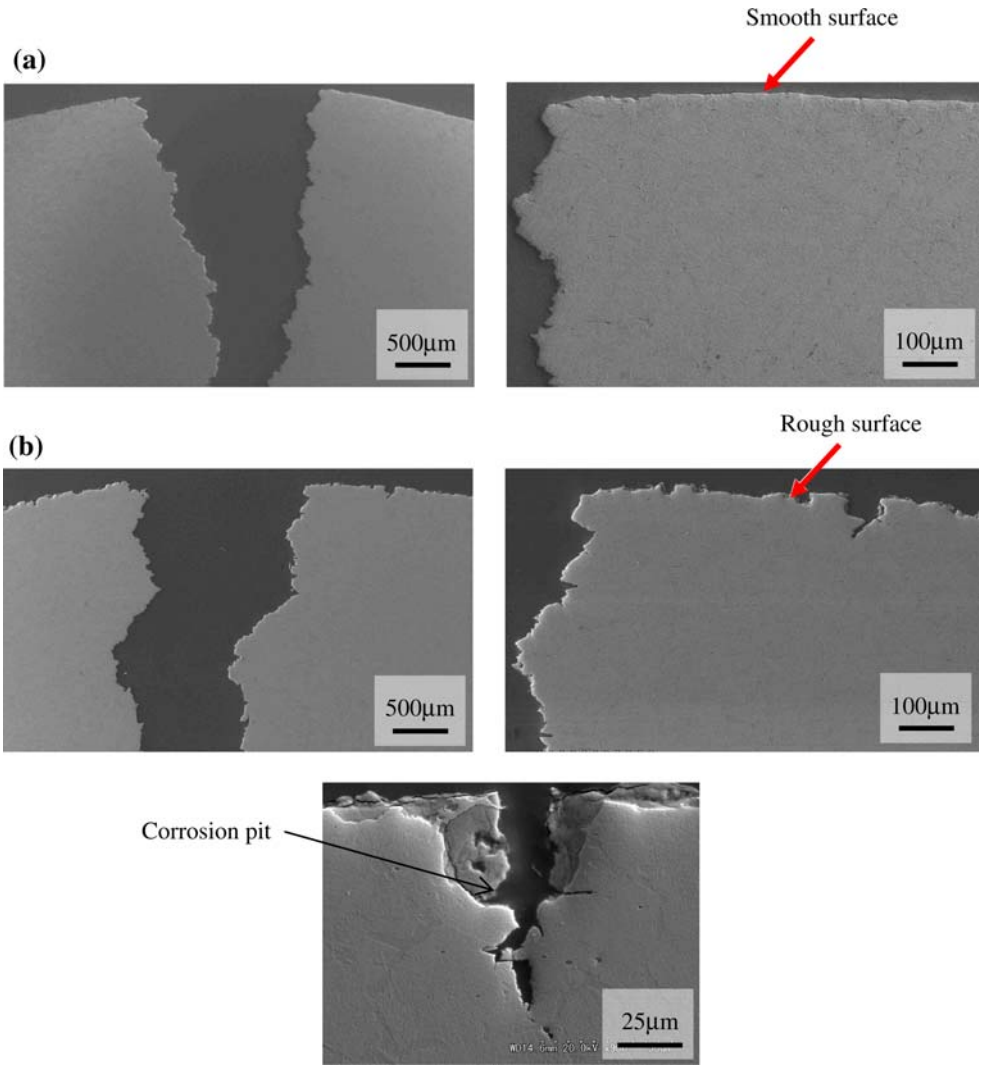

Fig. 7 SEM images of the cross section of the specimens showing fatigue cracks: **a** RC and **b** OC samples

and cathodic hydrogen reaction occurring by hydrogen permeation into the steel [3]. The Auger peak of carbon at 273 eV was also relatively high in the IC sample (1032KLL) compared to the other samples. In this case, the CO_2 and CH_4 cells, exhausted in the IC atmosphere, are attributed to chemical reaction with the sample. The chlorine AES at 180 eV was at a relatively high level in the OC sample (720LVV), which would be caused by NaCl in the sea breeze. On the other hand, a high sulfur AES level (1890LVV) was obtained for the RC sample, 4.4 times higher than that found for the IC and OC samples. Such a high sulfur level in RC would be related to the sulfur gas arising from the hot spring. From the above AES analysis, it could be substantiated that different corrosion system occurred, depending on the corrosion environment.

Bending and fatigue strengths

Figure 4 shows the bending properties of the uncorroded and corroded samples. It should be pointed out that the maximum deflection value was obtained from the point at which the sample is completely fractured. These results show that both the bending strength and deflection value for the as-received sample, 1784 MPa and 7.6 mm, are clearly higher than those for the corroded samples. Of the three corroded samples, the bending properties for OC and IC are similar but those of the RC samples are different. The bending strength for the RC sample (1428 MPa) is lower, but its deflection value (6.8 mm) is apparently higher than that for both the OC and IC samples. Such a change of the bending properties in the RC sample might be a result of the different corrosion system, and sulfur in the RC sample may have an important influence on its bending properties. In previous work, it was reported that iron sulfide, Fe_3S_2, causes the change of the fatigue strength [16] and sulfur and selenium could increase the material ductility [17]. The sulfur effects on the mechanical properties of the RC sample will be discussed in a later section of this paper.

Figure 5 represents the fatigue behavior (S–N relation) for all samples. As found for a conventional S–N diagram, the cycle number to failure increases with a decrease of the maximum bending stress. The mean endurance limit (σ_1) at 10^6 cycles for the uncorroded sample is about 925 MPa, which is equivalent to that for similar carbon steels [18, 19]. A considerable fall in the fatigue strength was found when the sample was corroded. As seen in Fig. 5, the fatigue strengths for all the corroded samples are reduced by more than 14%. The fatigue strengths of the IC and OC samples are similar even though the values are about 22% lower than that of the RC sample. The endurance limits at 10^6 cycles for the IC and OC samples are about 620 MPa, whereas for RC the figure is approximately 800 MPa. The high fatigue strength for RC might be associated with high material ductility, as shown in Fig. 4.

Failure characteristics

To understand the difference in the fatigue properties between RC, IC, and OC, a failure analysis was executed. Figure 6 shows SEM images of the cross section of each sample adjacent to the corrosion products. The rough surface with corrosion pits can be seen in both the IC and OC samples but a smooth surface is observed for the RC sample. Because of the different degrees of surface roughness, the stress concentration level may be altered [10, 20]. Figure 7 shows SEM micrographs of the RC and OC samples after being fractured by cyclic loading. As can be seen, different crack growth characteristics are obtained, e.g., the fatigue crack initiates from the corrosion pits in the OC sample but from everywhere in the smooth corroded surface of the RC sample.

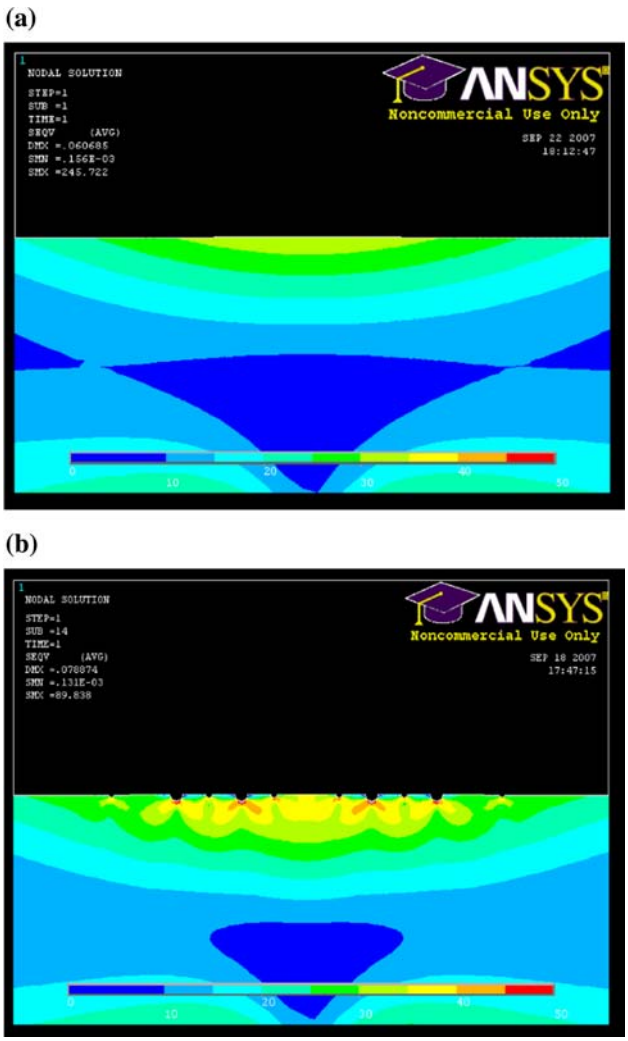

Fig. 8 von-Mises stress analysis for **a** RC and **b** IC (or OC) samples

To understand the effect of the surface morphology on the fatigue properties, an attempt was made to analyze the stress–strain distribution in the specimens around the corrosion products using FEA. Figure 8 presents the von-Mises stress distributions for the RC and IC samples. It should be pointed out that the morphology of the surface roughness in the models was designed on the basis of the actual surface shape. As seen in Fig. 8, different stress distributions were obtained; a high stress level is found in the area surrounding the corrosion pits for the IC sample but high stress cannot be seen in the RC sample. The different stress levels and their distribution may affect the change of fatigue strength shown in Fig. 5. Suresh has mentioned that "the formation of corrosion pits on the initially smooth surfaces of the fatigue specimen results in a significant reduction in the fatigue strength" [21].

To examine the fatigue behavior during cyclic loading, the variation of the deflection value as a function of the cycle number was examined. The results obtained for the uncorroded and OC samples are shown in Fig. 9a. In this case, all the deflection values were obtained from the low peak cyclic load collected by the data acquisition system. It is seen that the deflection value increases rapidly for the OC sample compared to the uncorroded one. Moreover, three distinct stages in the characteristic deflection versus cycle number are observed for both samples, with different crack growth characteristics, as presented in Fig. 9b. In Stage I, shear slip occurs in the specimen. In this case, the localized corrosion on the main slip plane of iron, e.g., {110}, may give rise to a high shear stress, resulting in the dislocation movement on that plane [5, 6]. In Stage II, the fatigue crack propagates with a constant rate, i.e., the Paris region of da/dN versus ΔK. The crack growth speed in Stage III then accelerates to failure. Similar crack growth stages have previously been reported [22].

Corrosion mechanism

As seen in Figs. 6 and 7, different surface morphologies were observed after the corrosion, e.g., RC versus IC (or OC). Such differences in the corrosion surface may be correlated with the different corrosion mechanisms. For example, water moisture from the river/hot spring could make a uniform thin layer on the surface of the RC specimen. This layer can give rise to a uniform degree of corrosion over the entire sample surface, resulting in a

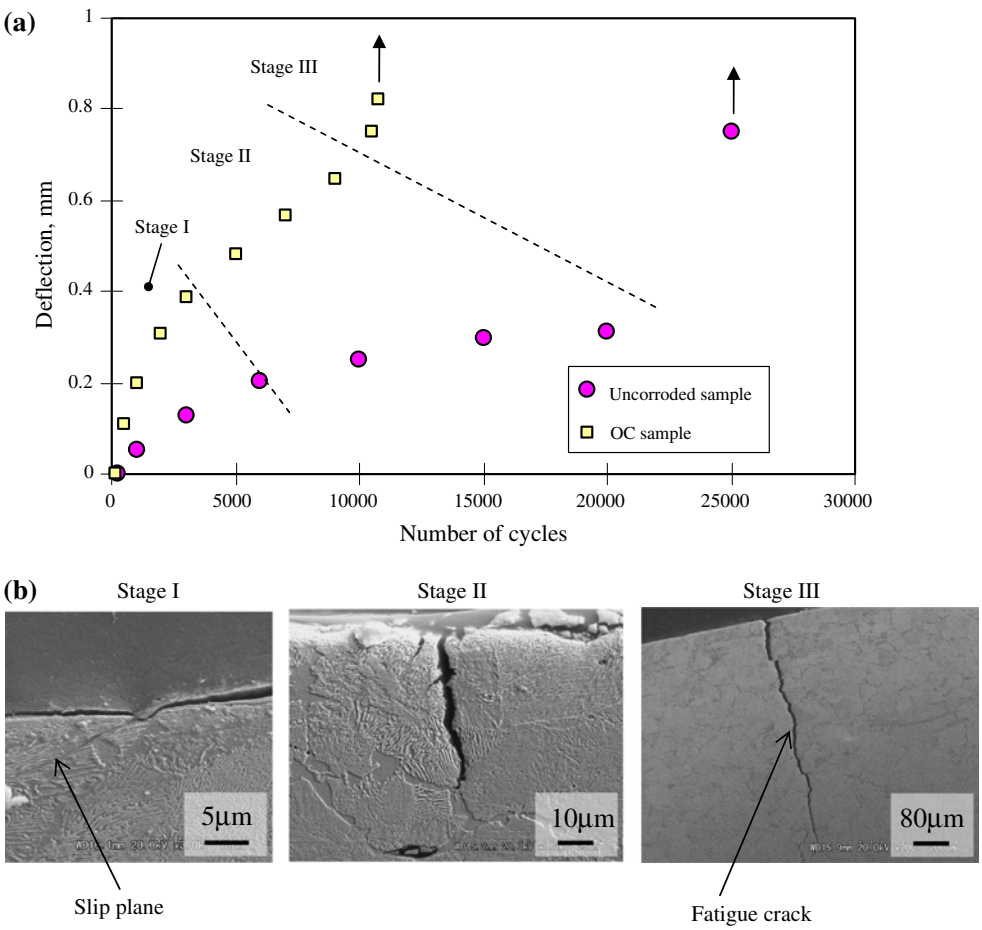

Fig. 9 **a** Deflection versus cycle number relationship for the uncorroded and OC samples; **b** SEM image of the cross section of the OC specimens showing shear slip and fatigue cracks

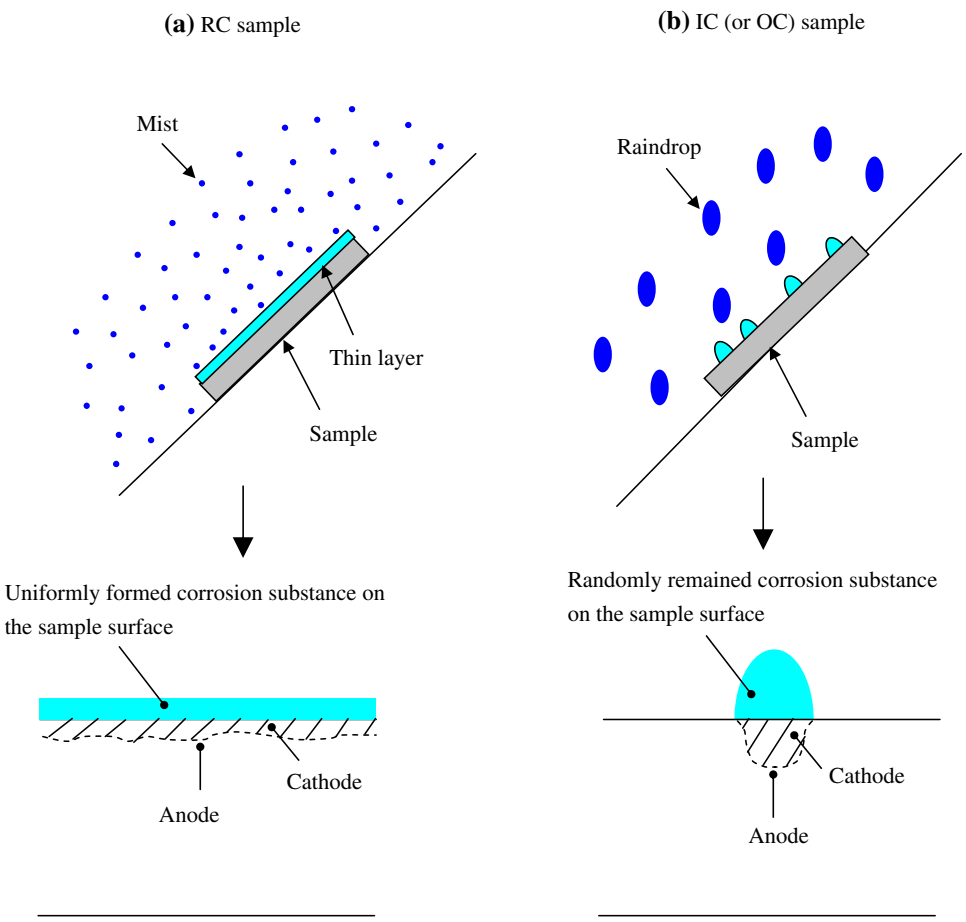

Fig. 10 Schematic illustration showing the corrosion mechanisms for **a** RC and **b** IC (or OC) samples

smooth face, as seen in Fig. 10a. On the other hand, the rough corrosion surfaces on the IC and OC specimens could be a consequence of highly localized corrosion (Fig. 10b), attributed to random small amounts of water on the sample. However, further clarification of these corrosion mechanisms will be required.

Fractography

Figure 11 presents SEM images of the fracture surfaces after the fatigue tests for (a) uncorroded sample, (b) RC sample, and (c) OC sample. Note that the fracture surface characteristics for IC and OC are similar. As seen, a discontinuous cleavage-like fracture [6] is obtained in the region near the specimen edge for the uncorroded and OC samples but a complicated fracture surface is seen in the RC sample. Interestingly, laminar corrosion products are obvious in the OC sample, as indicated by the white arrow in Fig. 11c. These may be influenced by the intergranular stress corrosion cracking [23]. Similar corrosion products are also clearly seen in the study by Even et al. [16]. In the theory of corrosion-fatigue in steels, the fundamental process is the penetration of a sufficiently large number of dislocations through the interface between the metal matrix and film substance [5, 22]. Unlike the laminar corrosion product, spiral- and meander-shaped corrosion products can be observed on the fracture surface of the RC sample, as seen in Fig. 11b. Since the meander-shaped corrosion products are detected in the sample not only near the surface but also inside the matrix (deep area) as enclosed by the white dotted circles, there could be severe corrosion in the RC sample compared to the IC and OC samples. This might also be related to the fact that a thick corrosion layer is obtained in the RC sample, about 6 times thicker than that for IC and OC, as mentioned previously. Due to the different corrosion characteristics, different bending and fatigue properties could be obtained, as shown in Figs. 4 and 5.

Conclusions

The effects of atmospheric corrosion on the fatigue properties of medium carbon steel have been investigated

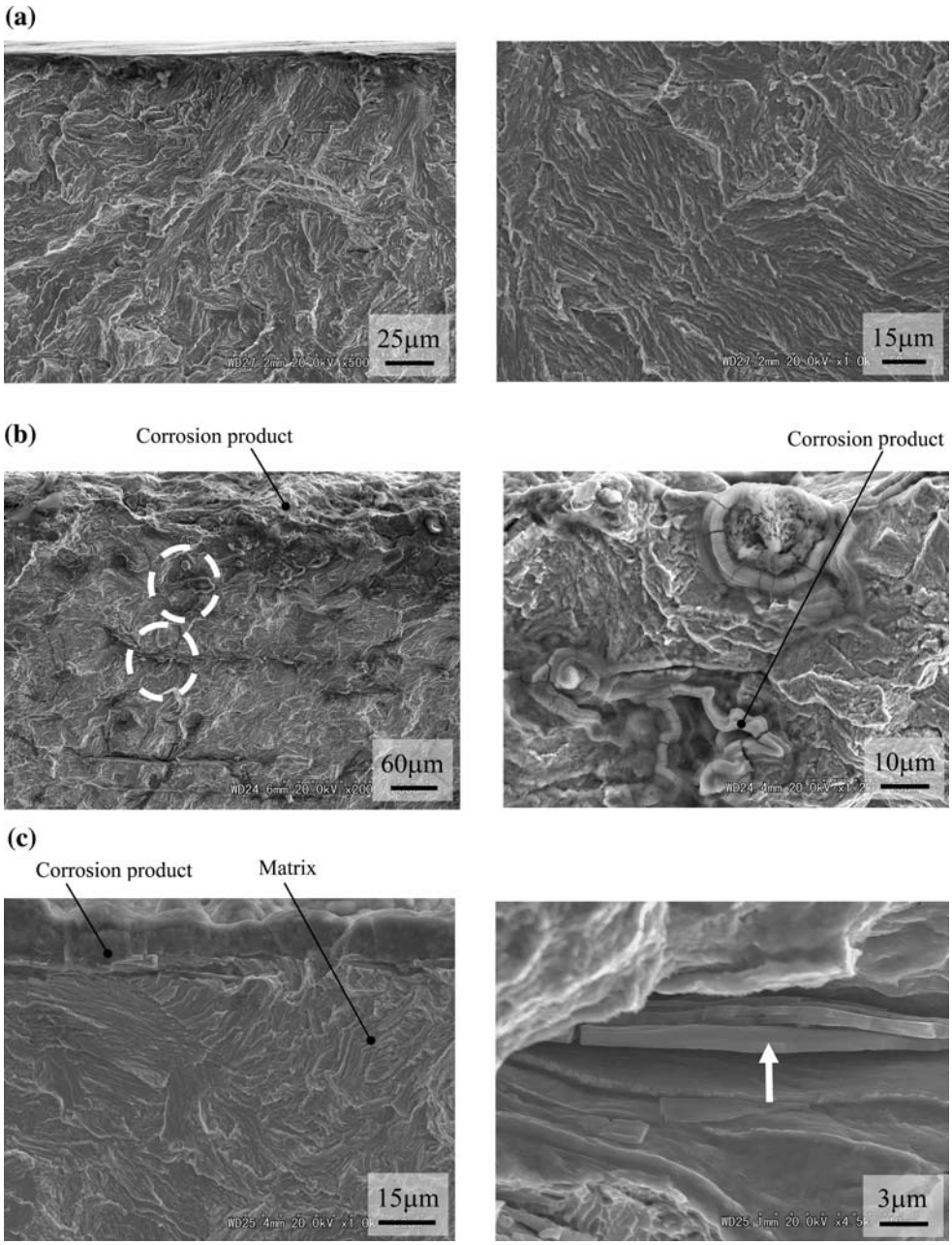

Fig. 11 SEM micrographs showing the fracture surface: **a** uncorroded, **b** RC, and **c** OC samples

experimentally. The corroded samples were prepared in three different places: (i) an industrial area, (ii) near the ocean and (iii) beside a river in a hot spring region. Based upon the experimental results and discussion above, the following conclusions can be drawn:

(1) Differences in corrosion characteristics are obtained depending on the location of corrosion. Strong corrosion by oxygen is detected in all samples. A high level of carbon is obtained for the IC sample, arising from CO_2 and CH_4 gases. The chlorine level is higher in the OC sample. This could be caused by NaCl from sea breezes. On the other hand, there is significant chemical reaction with sulfur in the RC sample due to the sulfur gas coming from the hot spring.

(2) The specimen surface morphology is altered by the corrosion. A smooth surface is created in the RC sample, but rough surfaces with corrosion pits are observed for the IC and OC samples. The change of the corrosion surface morphology could be explained by the following mechanism: a thin uniform water

layer forming on the sample surface makes a smooth corrosion face but randomly located corrosion substances on the specimen gives rise to a rough surface.

(3) The fatigue strength is directly affected by the surface morphology—the rougher the surface, the lower the fatigue strength. The mean endurance limit (σ_l) at 10^6 cycles for the RC samples is 800 MPa, which is approximately 1.3 times higher than that for the IC and OC samples.

(4) The material failure during fatigue tests occurs in three distinct stages. In Stage I, the deflection value increases via the plane slip or localized plastic deformation in the specimen. In Stage II, the fatigue crack propagates at a constant rate. The crack growth accelerates to failure in the final stage.

(5) The bending strength and the maximum deflection value for the uncorroded sample are higher than those for the corroded samples. Although the bending properties of the OC and IC samples are similar, those for RC are altered. The bending strength for the RC sample is lower than that for IC and OC, while the deflection value for RC is apparently higher. Such a high ductility for the RC sample could be a consequence of the high fatigue properties of RC.

(6) Corrosion occurs to a different extent depending on the sample. Because of strong corrosion, corrosion products are detected even in the deep matrix of the RC sample whereas for IC and OC these are seen only near the specimen edge (or corrosion layer). Such a change of corrosion characteristic could cause different bending and fatigue properties.

Acknowledgements This research was conducted under a special education program in Akita Prefectural University "Self-research program" for the 1st and 2nd year undergraduate students. This research work was financially supported by the government of Japan and Akita prefecture. Special thanks are due to Mr. Hajime Kudo (Tamagawa Hot-spring), Mr. Tokuji Sato (A. P. University), Ms. Miyuki Shibata (A. P. University), Mr. Hideaki Okayasu, and Ms. Ritsuko Okayasu for their technical support.

References

1. Karpenko GV, Litvin AK, Tkachev VI, Soshko AI (1975) Mater Sci 9:367
2. Moiseeva LS, Rashevskaya NS (2002) Russ J Appl Chem 75:1625
3. Fukuzumi T, Komazaki S, Misawa T (2002) Iron Steel Inst Jpn 88:31
4. Brass AM, Chêne J (2006) Corros Sci 48:3222
5. McEvily AJ, Wei RP (1971) In: International corrosion conference series; NACE-2, 14–18 June 1971, p 381
6. Magnin T, Chambreuil A, Chateau JP (1996) Int J Fract 79:147
7. Endo K, Komai K, Matsuda Y (1981) Bull Jpn Soc Mech Eng 24:1319
8. Komai K, Shikida T, Endo K (1985) Bull Jpn Soc Mech Eng 28:571
9. Dawson DB, Pelloux RM (1974) Met Trans 5:723
10. DuQuesnay DL, Underhill PR, Britt HJ (2003) Int J Fatigue 25:371
11. Dmytrakh IM, Pluvinage G, Qilafku G (2001) Mater Sci 37:184
12. Medved JJ, Breton M, Irving PE (2004) Int J Fatigue 26:71
13. Tokaji K, Ogawa T, Hwang JU, Kobayashi Y, Harada Y (1996) J Therm Spray Technol 5:269
14. Endo K, Komai K, Nkamuro N (1970) Bull Jpn Soc Mech Eng 13:837
15. Chitty JA, Pertuz A, Hintermann H, Puchi ES (1999) J Mater Eng Perform 8:83
16. Erven KA, Matlock DK, Krauss G (1991) J Heat Treat 9:27
17. Gol'dshtein YE, Zaslavskii AY, Guseva ZF (1973) Met Sci Heat Treat 15:286
18. Blokhin VK, Narusova EY, Livanova OV, Filippov GA (2003) Met Sci Heat Treat 45:10
19. Hanaki S, Goto H, Yamashita M, Uchida H (2006) J Soc Mater Sci, Jpn 55:1011
20. Callister WD Jr (2007) Materials science and engineering, 7th edn. Wiley, Hoboken, NJ, p 237
21. Suresh S (2004) Fatigue of materials, 2nd edn. Cambridge University Press, New York, p 157
22. Schoch W, Spahn H (1971) In: International corrosion conference series; NACE-2, 14–18 June 1971, p 52
23. Shibata T (2006) J Soc Mater Sci Jpn 55:979